**⟲AGU**PUBLICATIONS

*Geophysical Research Letters*

Supporting Information for

**Modulation of mid-Holocene African rainfall by dust aerosol direct and indirect effects**

Alexander J. Thompson[1], Christopher B. Skinner[1,2], Christopher J. Poulsen[1], and Jiang Zhu[1]

[1]Department of Earth and Environmental Sciences, University of Michigan, Ann Arbor, Michigan, USA, [2]Department of Environmental, Earth and Atmospheric Sciences, University of Massachusetts Lowell, Lowell, MA, USA

Corresponding author: Alexander J. Thompson (alexjt@umich.edu)

**Contents of this file**

Text S1 to S3
Figures S1 to S10
Tables S1 to S4

**Introduction**

This supporting document includes a description of model dust properties, (Text S1), the offline radiative transfer calculation method (Text S2), a definition of the northern limit of the West African Monsoon (Text S3), ten supplementary figures, and four supplementary tables. Figure S1 shows the setup of prescribed vegetation used in the simulations. Figure S2 displays the differences in temperature, geopotential height, and winds between the *MH Control* and *PI Control* simulations. Figure S3 displays precipitation and northern monsoon limits for each of the six simulations performed. Figure S4 shows simulated dust aerosol optical depth (AOD) for each of the six simulations. Figure S5 illustrates radiative and heat fluxes due to dust. Figure S6 exhibits atmospheric profiles for cloud variables averaged over the Sahel. Figure S7 shows an atmospheric profile of Saharan and Sahel aerosol absorption. Figure S8 indicates temperature and stratus cloud changes from a sensitivity experiment with darker soil. Figure S9 demonstrates the precipitation increase from a sensitivity experiment with expanded vegetation cover. Figure S10 illustrates a model-proxy comparison. Table S1 and Table S2 provide additional boundary condition details. Table S3 displays single-scatter albedo. Table S4 shows net Saharan radiative fluxes.

**Text S1.**

In CAM5-chem, aerosols are predicted with the three-mode version of the Modal Aerosol Module. The size range for dust bins is 0.1-1.0 µm in accumulation mode and 1.0-10 µm in coarse mode. Aerosol radiative properties (e.g. single-scatter albedo) are a function of wet refractive index and wet surface radius (Neale et al., 2012).

**Text S2.**

To isolate the direct aerosol effect associated with reduced Saharan dust, offline radiative transfer calculations were performed following the methodology of Colman (2003) with the parallel offline radiative transfer (PORT) tool (Conley et al., 2013). This method calculates radiative perturbations caused by a Saharan dust reduction, while keeping other radiation-related fields (e.g., temperature, water vapor, and clouds) unchanged. We conducted two control offline radiation calculations for *MH Control* and *MH HighDust*, respectively, with high frequency output of radiation-related fields. We then performed a sensitivity offline radiation calculation of the *MH Control* case with only the dust aerosol fields substituted by those from *MH HighDust*. The radiation perturbation was diagnosed as the difference between the sensitivity and *MH Control* offline radiation calculations. To ensure the offline radiation calculation reproduced the online version in CAM5-chem, 6-hourly radiation fields were used. To reduce potential interannual variation, the offline radiation calculation was conducted for five years for each case, with the last four used in analysis.

**Text S3.**

      To define the northern limit of the West African Monsoon (WAM), we use a threshold of 2 mm/day, adapted from 60 mm/month, averaged over the zonal region 15°W–20°E (Pausata et al., 2016). With monthly model output, we calculate the northernmost latitude that exceeds 2 mm/day for each month over the zonal region. We find the northernmost latitude for each year, taken as the maximum of the year's monthly values, and create a distribution of northernmost latitudes for each of the 30 simulated years. The median value of each respective simulation's 30-year distribution is determined as the northernmost latitude the WAM reaches in that simulation. Like Pausata et al. (2016), we use the median, as opposed to the mean, because it uses percentiles and is not affected by the shape of the distribution.
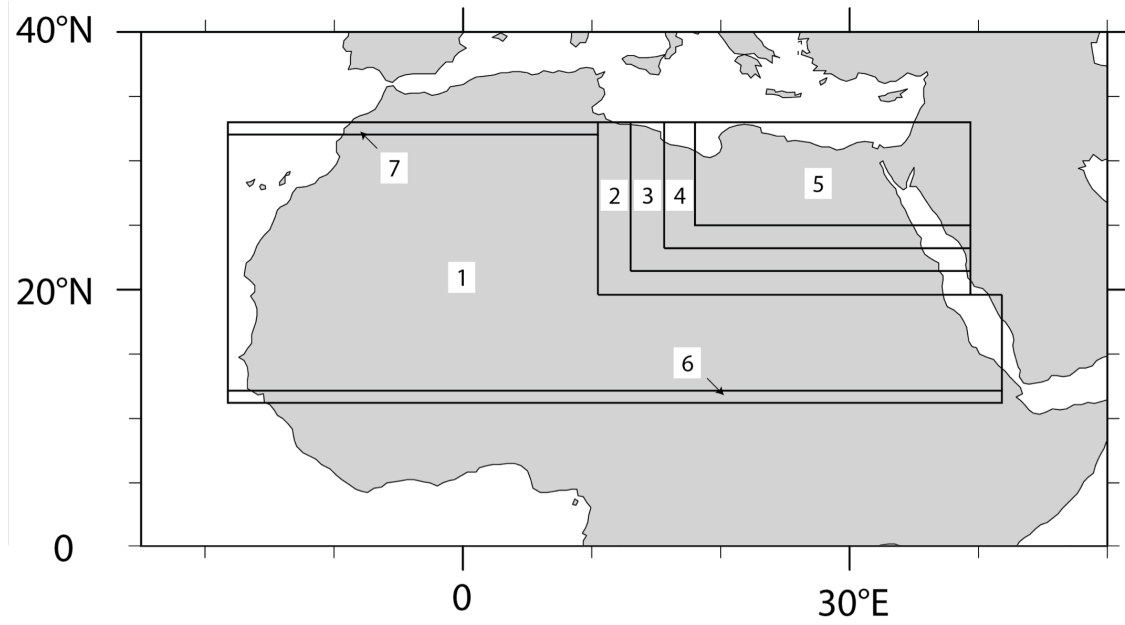
**Figure S1.** Mid-Holocene prescribed land surface zones. Details regarding plant functional type, leaf area index, and soil albedo specifications for each numbered zone are listed in Table S2.
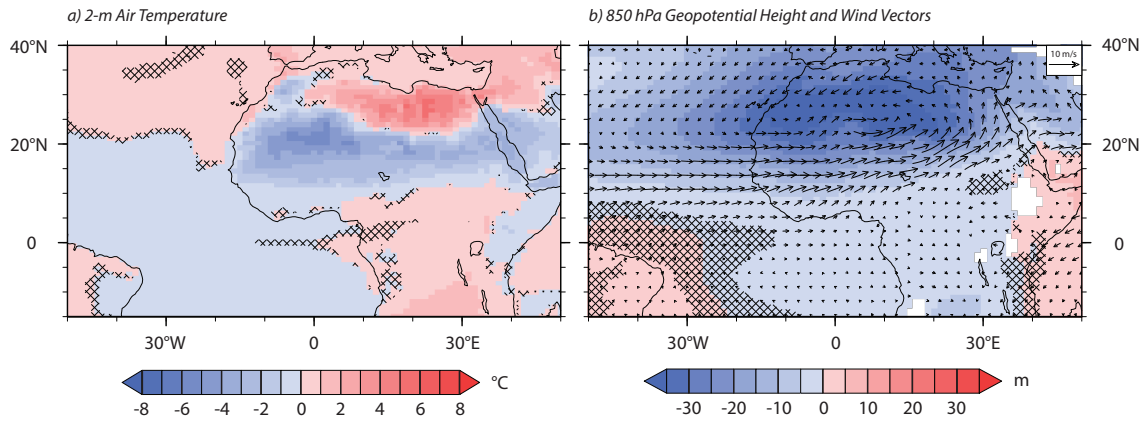
**Figure S2.** Difference (*MH Control – PI Control*) in monsoon season (JJAS) a) 2-m air temperature and b) 850 hPa geopotential height and winds. Differences that are not significant at the 95% confidence level are shown by cross-hatching.
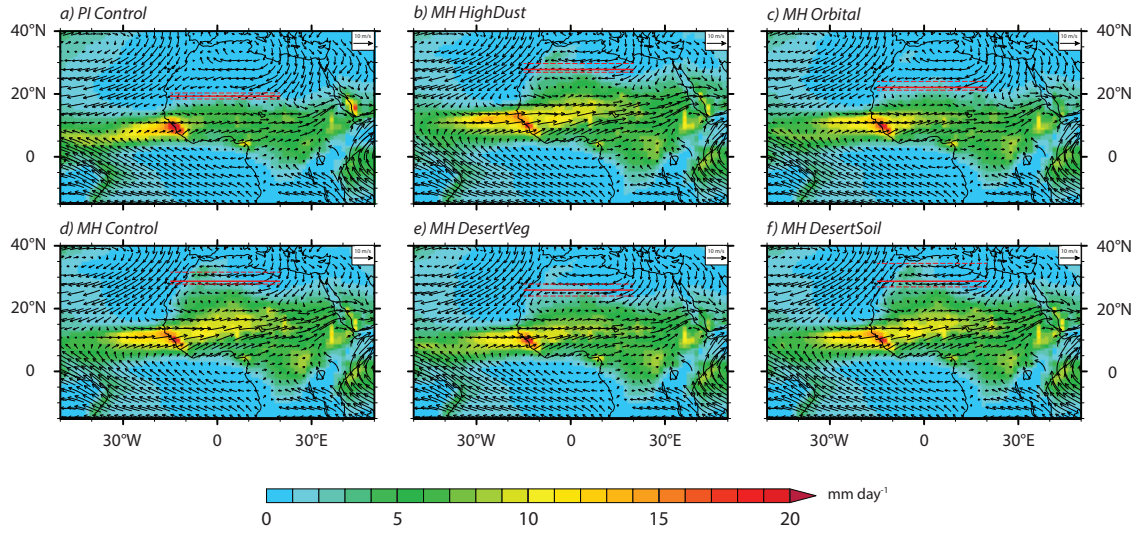
**Figure S3.** Monsoon season (JJAS) total precipitation and 850 hPa wind vectors for a) *PI Control*, b) *MH HighDust*, c) *MH Orbital*, d) *MH Control*, e) *MH DesertVeg*, and f) *MH DesertSoil* simulations. Solid red line represents the median northernmost latitude reached by the West African Monsoon (WAM) throughout the 30-year simulations. Dashed lines above and below the median latitude represent 75th and 25th percentile latitudes, respectively.
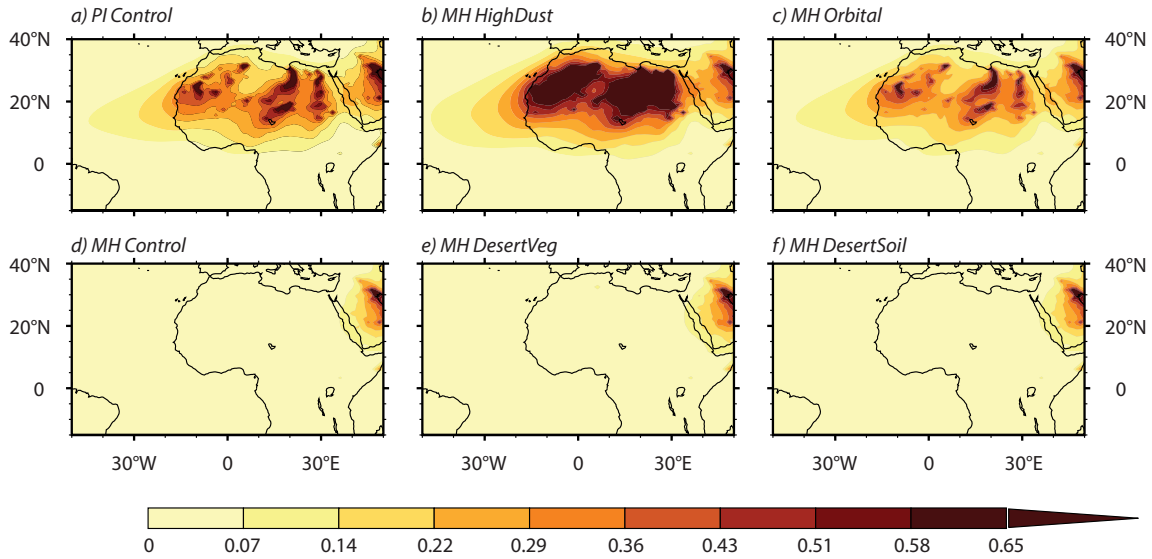
**Figure S4.** Annual dust aerosol optical depth (AOD) for a) – f) each CESM CAM5-chem simulation. Comparison of a) and b) with dust output from EC-Earth simulations in Pausata et al. (2016) and Gaetani et al. (2017) (see Gaetani et al. (2017), Figures S1a and S1b) demonstrates that CAM5-chem more closely captures the present-day dust distribution in the western Sahara. Note also that the increased dust AOD in b) compared with c) occurs due to stronger monsoon flow from expanded vegetation cover.
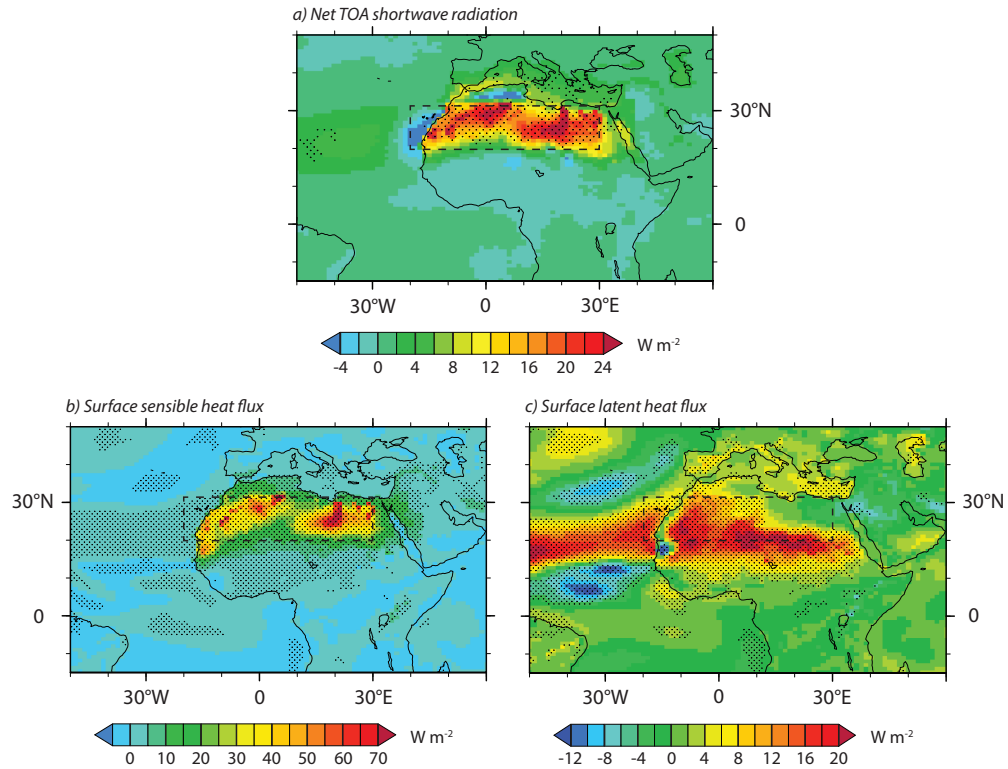
**Figure S5.** Monsoon season (JJAS) difference (*MH Control – MH HighDust*) for a) net shortwave radiative flux at TOA, b) surface sensible heat flux, and c) surface latent heat flux. a) represents radiative differences due to direct dust aerosol effects only from offline radiation calculations. b) and c) incorporate all radiative effects and feedbacks. Positive differences represent a net downward flux for a) and upward flux for b) and c). Stippling represents statistically significant differences at the 95% confidence level.
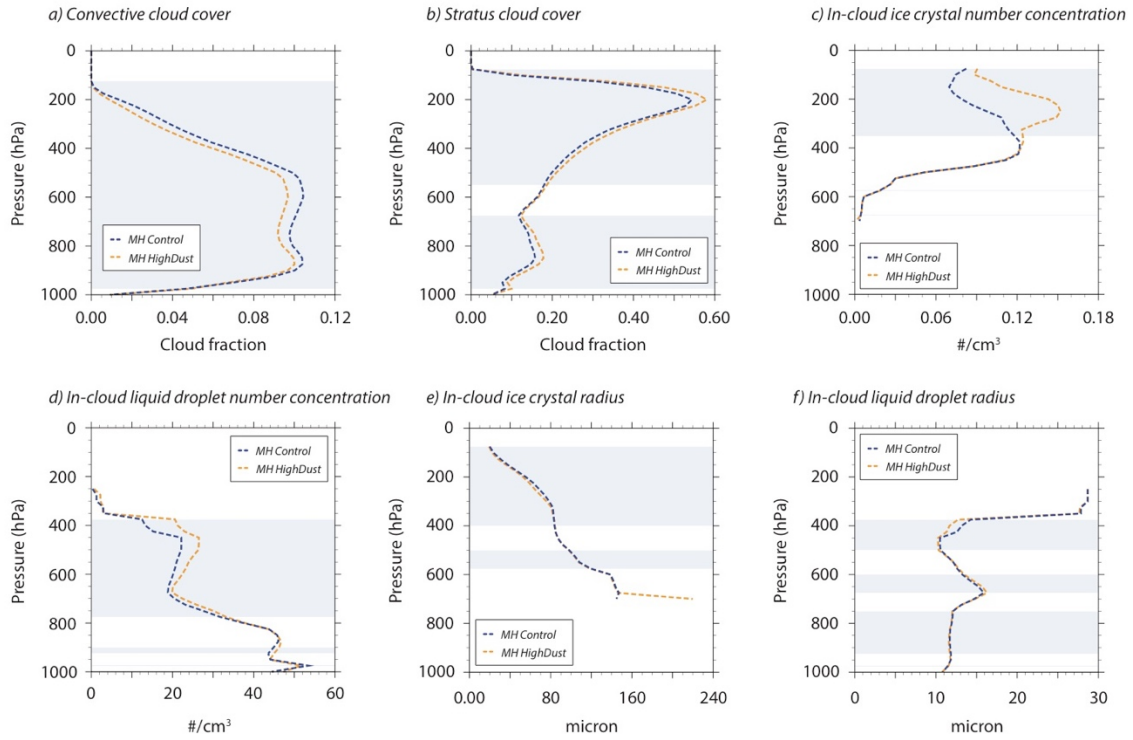
**Figure S6.** Monsoon season (JJAS) Sahel-averaged (10–20°N, 15°W–30°E) atmospheric profiles for *MH Control* and *MH HighDust* for a) convective cloud cover, b) stratus cloud cover, c) in-cloud ice crystal number concentration, d) in-cloud liquid droplet number concentration, e) in-cloud ice crystal radius, and f) in-cloud liquid droplet radius. Blue shading indicates statistically significant differences at the 95% confidence level. "In-cloud" variables are calculated by dividing the specified model output variable (i.e. ice crystal number concentration) by the fractional occurrence of ice or liquid.
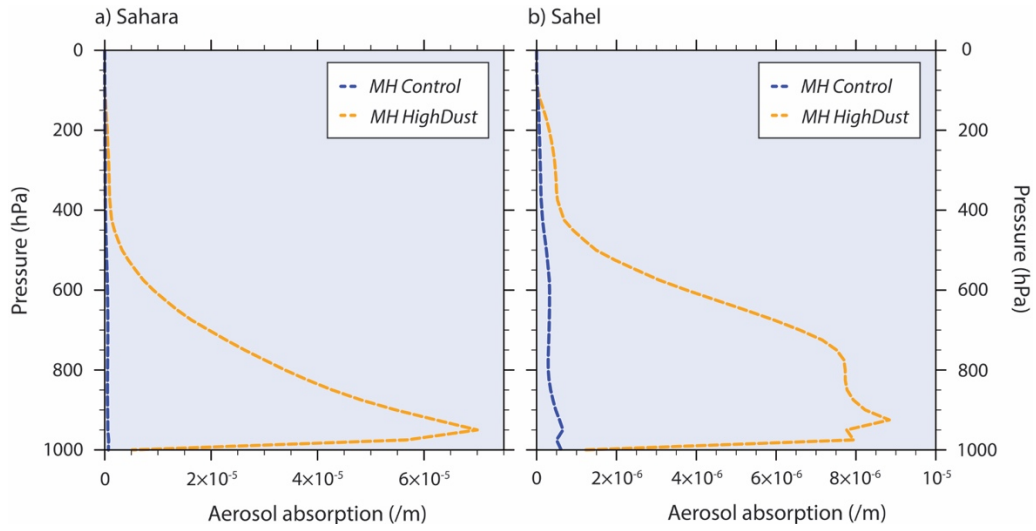
**Figure S7.** Monsoon season (JJAS) a) Saharan-averaged and b) Sahel-averaged atmospheric profile of aerosol absorption for *MH Control* and *MH HighDust*. Differences are statistically significant at the 95% confidence level at all levels.
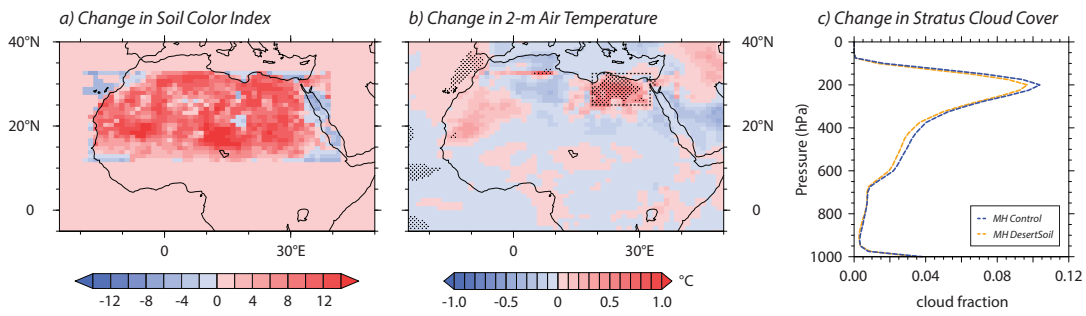
**Figure S8.** Sensitivity experiment with darker soil (*MH Control – MH DesertSoil*) showing a) change in soil color index (no units), b) the corresponding change in monsoon season (JJAS) 2-m air temperature, and c) the JJAS atmospheric profile of stratus cloud cover over the dashed region of surface warming in b) (25–32.5°N, 18.75°–32.5°E). For a), red values represent simultaneous decreases in albedo and increases in soil darkness. An increase in soil color index of 12, as exhibited across much of the Sahara, is representative of a decrease in dry and saturated albedo of ~0.14 and ~0.13, respectively. For example, this change could occur with a shift from Color Class 2 to Color Class 14 as shown in Table 3.3 of Oleson et al. (2010), which displays the dry and saturated albedo values associated with each index in CLM4.0. For b) and c), we highlight the region of warming in the northeastern Sahara because its prescribed vegetation (grassland) allows for greater interaction between the soil and solar radiation than the prescribed vegetation throughout the rest of the Sahara (mostly denser shrub). Thus, the change in soil albedo warms the surface here, while it has no significant effect on the remainder of the Sahara. Stippling in b) represents statistically significant differences at the 95% confidence level. The values in c) are not statistically significant at the 95% confidence level, but do illustrate a weak increase in stratus cloud cover throughout much of the atmospheric column.

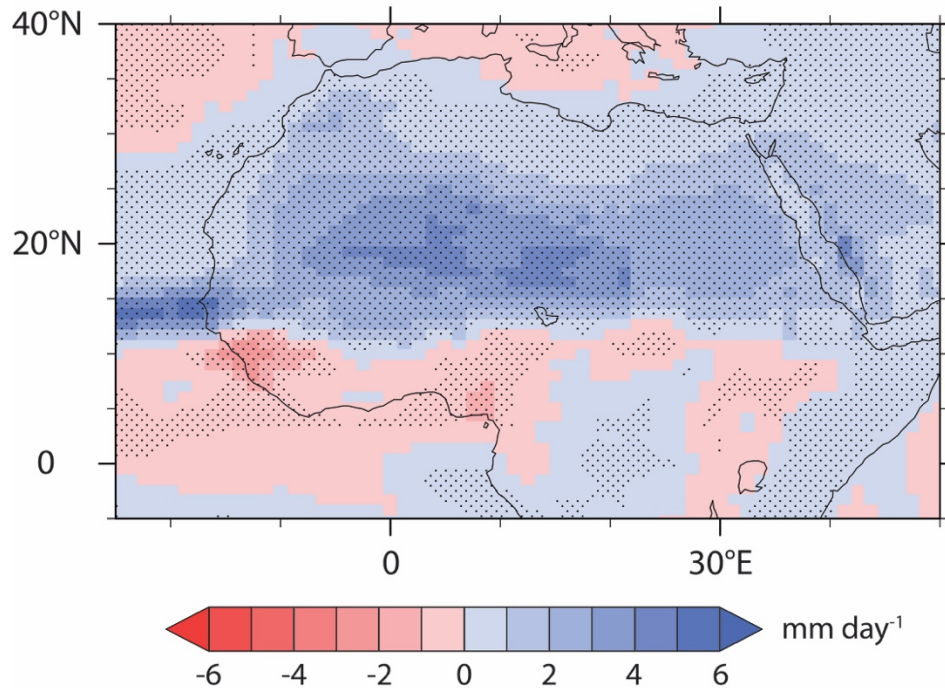**Figure S9.** Monsoon season (JJAS) total precipitation from sensitivity experiment with expanded vegetation cover (darker surface albedo) and no reduction in dust (*MH HighDust – MH Orbital*). Stippling represents statistically significant differences at the 95% confidence level. To test difference in rainfall response to vegetation albedo changes without a reduction in dust, compare this figure to Figure 5b from Pausata et al. (2016).
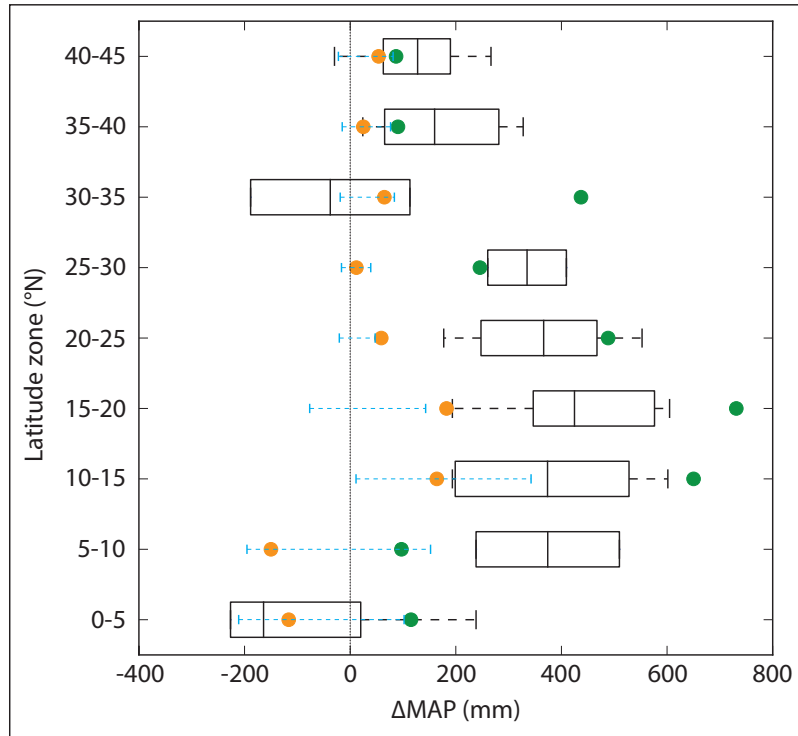
**Figure S10.** Changes in mean annual precipitation (MAP) from climate model simulations and reconstructions for 5° latitude bands between 20°W–30°E. Data for the reconstructions are from Bartlein et al. (2011) and are displayed as boxplots, which include the mean, 25% and 75% quartiles, and full range. Boxplots are calculated from available Bartlein et al. (2011) data points within each latitudinal band. CAM5-chem model results from this paper are shown by green dots (*MH Control – PI Control*) and orange dots (*MH Orbital – PI Control*). The full range of mid-Holocene PMIP3 model results (MH – PI) from Perez-Sanz et al. (2014) are shown as blue dashed lines. For both CAM5-chem and PMIP3, the results are calculated for the grid cells with available data in Bartlein et al. (2011). This figure is adapted from Fig. 6 in Perez-Sanz et al. (2014).

**Table S1.** Greenhouse gas concentrations, orbital parameters, and dust boundary conditions for simulations of Preindustrial (PI) and mid-Holocene (MH) time periods.

| Time Period | CH$_4$ | Eccentricity | Obliquity | Precession | Dust emissions |
|---|---|---|---|---|---|
| Preindustrial (PI) | 791.6 ppb | 0.016724 | 23.446° | 102.04° | Mobilized over Sahara |
| Mid-Holocene (MH) with PI vegetation | 650 ppb | 0.018682 | 24.105° | 0.87° | Mobilized over Sahara[a] |
| Mid-Holocene (MH) with MH vegetation | 650 ppb | 0.018682 | 24.105° | 0.87° | Not mobilized over Sahara[a] |

[a]Unless stated otherwise in Model Experiments and Methods.

**Table S2.** Mid-Holocene prescribed land surface characteristics for each zone. Numbered zones correspond with Figure S1.

| Zone | Plant functional types | Leaf area index | Soil albedo |
|------|------------------------|-----------------|-------------|
| 1 | 100% Broadleaf evergreen temperate shrub | Broadleaf evergreen temperate shrub = 2.6 | 0.18 (dry) - 0.09 (saturated) |
| 2 | 75% Broadleaf evergreen temperate shrub, 25% Warm c4 grass | Broadleaf evergreen temperate shrub = 2.6; Warm c4 grass = 0.33 (Jan-Apr), 1.0 (May-Dec) | 0.18 (dry) - 0.09 (saturated) |
| 3 | 50% Broadleaf evergreen temperate shrub, 50% Warm c4 grass | Broadleaf evergreen temperate shrub = 2.6; Warm c4 grass = 0.33 (Jan-Apr), 1.0 (May-Dec) | 0.20 (dry) - 0.10 (saturated) |
| 4 | 25% Broadleaf evergreen temperate shrub, 75% Warm c4 grass | Broadleaf evergreen temperate shrub = 2.6; Warm c4 grass = 0.33 (Jan-Apr), 1.0 (May-Dec) | 0.22 (dry) - 0.11 (saturated) |
| 5 | 100% Warm c4 grass | Warm c4 grass = 0.33 (Jan-Apr), 1.0 (May-Dec) | 0.22 (dry) - 0.11 (saturated) |
| 6 | 20% Bare, 40% Warm c4 grass, 34% Broadleaf evergreen temperate shrub, 3% Broadleaf deciduous tropical tree, 3% Cool c3 grass | Bare = 0, Broadleaf deciduous tropical tree = 0.87 (Jan-Apr), 2.6 (May-Dec); Cool c3 grass = 0.33 (Jan-Apr), 1.0 (May-Dec); Warm c4 grass = 0.33 (Jan-Apr), 1.0 (May-Dec); Broadleaf evergreen temperate shrub = 2.6 | 0.22 (dry) - 0.11 (saturated) |
| 7 | 57% Bare, 40% Broadleaf evergreen temperate shrub, 3% Broadleaf deciduous temperate shrub | Bare = 0; Broadleaf deciduous temperature shrub = 0.87 (Jan-Apr), 2.6 (May-Dec); Broadleaf evergreen temperate shrub = 2.6 | 0.23 (dry) - 0.12 (saturated) |

**Table S3.** Monsoon season (JJAS) Saharan-averaged values for single-scatter albedo for each simulation. In CAM5-chem, aerosol single-scatter albedo is predicted as a function of wet refractive index and wet surface radius (Neale et al., 2012). Lower values represent aerosols with greater absorption and higher values represent aerosols with weaker absorption. Values differ between simulations due to the amount of aerosol over the Sahara.

| Simulation | Single-scatter albedo |
|---|---|
| *PI Control* | 0.887 |
| *MH Control* | 0.950 |
| *MH HighDust* | 0.884 |
| *MH DesertVeg* | 0.942 |
| *MH DesertSoil* | 0.949 |
| *MH Orbital* | 0.887 |

**Table S4.** Offline radiation calculations of changes in average monsoon season (JJAS) net radiative fluxes at the surface and the top-of-atmosphere (TOA) over the Sahara (20–31°N, 20°W–30°E) due to MH dust reductions. Here offline calculation was used to separate the direct aerosol effects from the total radiation changes after accounting for feedbacks in the system (e.g., clouds, temperature, and water vapor). For comparison, total changes in radiation, including both direct aerosol effects and feedbacks, are shown in the bottom row.

| | | Difference (*MH Control – MH HighDust*) (W m$^{-2}$) |
|---|---|---|
| Surface (direct aerosol effects)[b] | SW | +67.4 |
| | LW | +17.3 |
| | Total[a] | +84.7 |
| TOA (direct aerosol effects)[b] | SW | +13.7 |
| | LW | -4.8 |
| | Total[a] | +8.9 |
| TOA (total = direct aerosol effects + feedbacks)[b] | SW | +16.5 |
| | LW | -18.4 |
| | Total[a] | -1.9 |

[a]Shortwave flux + Longwave flux = Total flux. [b]Positive values represent downward flux.